Lithos 184–187 (2014) 314–323

Contents lists available at ScienceDirect

Lithos

journal homepage: www.elsevier.com/locate/lithos

Geochronology, petrogenesis and tectonic significance of the Jitang granitic pluton in eastern Tibet, SW China

Yan Tao [a,*], Xianwu Bi [a], Chusi Li [b], Ruizhong Hu [a], Yubang Li [a,c], Mingyang Liao [a,c]

[a] State Key Laboratory of Ore Deposit Geochemistry, Institute of Geochemistry, Chinese Academy of Sciences, Guiyang, 550002, China
[b] Department of Geological Sciences, Indiana University, Bloomington, IN 47405, USA
[c] University of Chinese Academy of Sciences, Beijing 100049, China

ARTICLE INFO

Article history:
Received 27 March 2013
Accepted 26 October 2013
Available online 5 November 2013

Keywords:
Zircon dating
S-type granite
Sr–Nd isotopes
Crustal anatexi
Qiangtang
Gondwana

ABSTRACT

The Jitang granitic pluton, which is situated in the southern margin of the North Qiangtang block in eastern Tibet, may provide critical information about the source and derivation of the North Qiangtang block during Gondwana breakup and dispersion. In this paper we report relevant data such as zircon U–Pb age, whole-rock major and trace element abundances, and Sr–Nd isotopes for the Jitang pluton. The major rock types of the pluton are granodiorite and biotite granite. Whole-rock major element data reveal that the Jitang pluton is a peraluminous S-type granitic pluton. The U–Pb age of zircons from the pluton is 219.1 ± 1.7 Ma, which is ~10 Ma younger than the age of high-pressure metamorphism in the Longmu Co–Shuanghu collisional suture between the North and South Qiangtang blocks. The Jitang granitoids show pronounced negative Ba–Eu–Sr anomalies, high initial $^{87}Sr/^{86}Sr$ ratios from 0.7266 to 0.7389 and low $\varepsilon_{Nd}(t)$ values for from −11.1 to −13.2, which are remarkably similar to the gneisses and meta-sedimentary rocks from the Indian craton as well as the North Qiangtang block. The results from this study indicate that the Jitang granitoids formed by melts derived from a crustal source with Sr–Nd isotopic compositions similar to those of the Indian cratonic crust. We concur with the previous interpretation based on detrital zircon records that the North Qiangtang block was derived from the Indian Gondwana.

1. Introduction

The Sanjiang (Jinshajiang, Lancangjiang and Nujiang) region in eastern Tibet and Yunnan province is a collage of Gondwana-derived micro-continents, Paleozoic arc terranes and the remnants of Tethys oceans (Deng et al., 2013; Metcalfe, 2013; Yin and Harrison, 2000; Zhu et al., 2013). The different continental blocks are separated by sub-parallel suture zones stretching over 1000 km from Tibet to Yunnan, SW China (Fig. 1a). Among all of the micro-continental blocks in this region, the derivation of the Simao and North Qiangtang blocks is most enigmatic. Some researchers have suggested that the two micro-continental blocks were derived from the South China block based on Permian bio-strata correlation (Metcalfe, 2002, 2013; Zhang et al., 2013). Other researchers have proposed that they were derived from the Indian Gondwana based on detrital zircon records (He et al., 2011; Pullen et al., 2008; Usuki et al., 2012; Wang et al., 2013; Zhu et al., 2013). Triassic granitoids within the Simao and North Qiangtang blocks such as the Lincang batholith and the Jitang pluton may provide important information about the derivation of the micro-continental blocks during Gondwana breakup and dispersion, because different crustal sources commonly have different trace element and Sr–Nd isotope signatures. For this purpose we have carried out an integrated geochronological, petrological and geochemical study of the Jitang granite pluton which occurs in the southern margin of the North Qiangtang block, eastern Tibet (Fig. 1b).

2. Geological background

Abundant granitoids including the Jitang pluton and the Lincang batholith occur along the Longmu Co–Shuanghu collisional suture between the North and South Qiangtang blocks in eastern Tibet and along the Changning–Menglian collisional suture between the Simao and Baoshan blocks in Yunnan province, respectively (Fig. 1b). There is a general consensus that the micro-continental blocks on the south or west side of these sutures were derived from the Australian Gondwana (Deng et al., 2013; Metcalfe, 2013; Zhu et al., 2013). The micro-continental blocks on the north or east side of the sutures may have been derived from the Indian Gondwana (He et al., 2011; Pullen et al., 2008; Usuki et al., 2012; Zhu et al., 2013) or from the South China block (Metcalfe, 2002, 2013; Zhang et al., 2013).

Available geochronological data show that most of the granitic plutons in the Simao and North Qiangtang blocks are contemporaneous, with ages varying between 210 and 230 Ma. For examples, the Rongma granite pluton along the western segment of the Longmu Co–Shuanghu suture has an Ar–Ar age of ~215 Ma (Liu et al., 2011), the Dongdashan

* Corresponding author.
E-mail address: taoyan@vip.gyig.ac.cn (Y. Tao).

0024-4937/$ – see front matter © 2013 Elsevier B.V. All rights reserved.
http://dx.doi.org/10.1016/j.lithos.2013.10.031

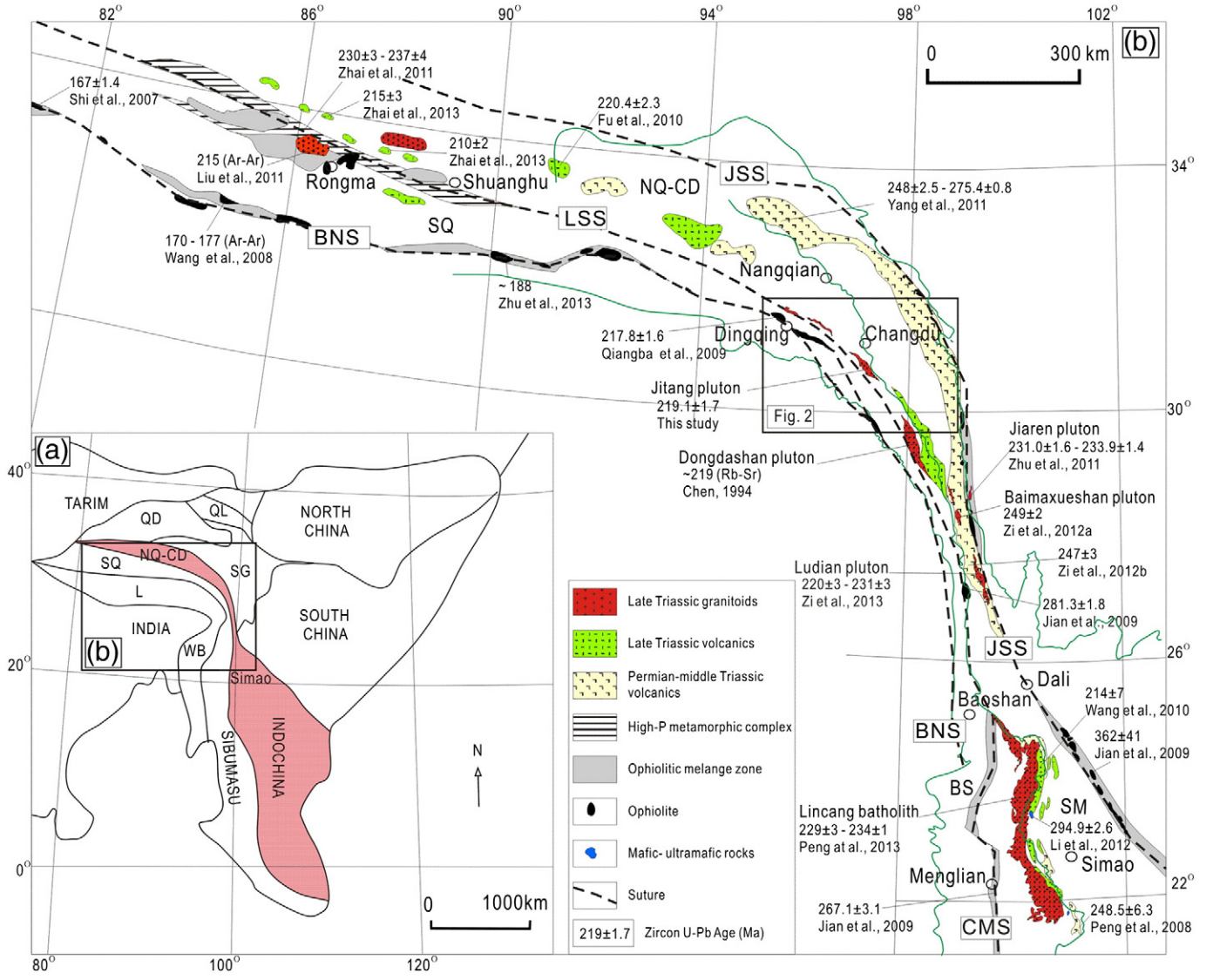

Fig. 1. Continental blocks of SE Asia (a) and simplified geological map of eastern Tibet and Sanjiang region (b) (modified from Li et al., 2012; Deng et al., 2013; Zhu et al., 2013. The ages are from Fu et al., 2010; Jian et al., 2009 ; Qiangba et al., 2009; Shi, 2007; Wang et al., 2008; Wang et al., 2010; Zhai et al., 2013; Zhu et al., 2011; Zi et al., 2013; etc. as showing in the figure). Sutures: *JSS*, Jinshajiang suture; *LSS*, Longmu Co–Shuanghu suture; *CMS*, Changning–Menglian suture; *BNS*, Bangong–Nujiang suture. Continental blocks: *NQ*, North Qiangtang; *SM*, Simao; *SQ*, South Qiangtang; *BS*, Baoshan; *WB*, West Burma; *L*, Lhasa; *SG*, Songpan Ganzi; *QD*, Qaidam; *QL*, Qilian.

granitic pluton along the eastern segment of the Longmu Co–Shuanghu suture has a Rb–Sr isochron age of ~219 Ma (Chen et al., 1994), the Lincang batholith along the Changning–Menglian suture zone has zircon U–Pb ages from ~210 to ~230 Ma (Dong et al., 2013; Peng et al., 2006, 2013). Abundant granitoids with slightly older ages occur along the Jinshajiang suture to the east (Fig. 1b). For examples, the zircon U–Pb ages of the Baimaxueshan and Ludian granitic plutons along the Jinshajiang suture are 249 ± 2 Ma (Zi et al., 2012a) and 247 ± 3 Ma (Zi et al., 2012b), respectively. The Baimaxueshan pluton is a I-type granite pluton with moderate initial $^{87}Sr/^{86}Sr$ ratios from 0.710 to 0.711 and $\varepsilon_{Nd}(t)$ values from −8 to −9.5 (Zi et al., 2012a). In contrast, the younger Lincang batholith is an S-type granite pluton with much higher initial $^{87}Sr/^{86}Sr$ ratios from 0.724 to 0.741 and slightly lower $\varepsilon_{Nd}(t)$ values from −11 to −14 (Hennig et al., 2009; Peng et al., 2013).

The Jitang pluton is located in the eastern segment of the Longmu Co–Shuanghu suture in the Changdu region. In this region, Proterozoic meta-sedimentary rocks including gneissic rocks of the Jitang group are present along the suture (Fig. 2). They are overlain by Triassic volcanic rocks, which in turn are overlain by younger sedimentary rocks. During the India–Asia collision in the past 65 Ma, the Changdu region had undergone strong shearing and over-thrusting (Burchfiel and Chen, 2012; Yin and Harrison, 2000). Small Cenozoic granitic porphyry bodies are present close to the suture, farther to the north within the North Qiangtang block (Bi et al., 2009; Liang et al., 2009).

The middle segment of the Longmu Co–Shuanghu suture near Rongma is marked by a prominent high-P metamorphic belt (Fig. 1b). The U–Pb ages of zircons from the eclogites of this belt are between 230 and 237 Ma (Zhai et al., 2011). These ages are thought to represent the timing of continental collision between the South and North Qiangtang blocks (Zhai et al., 2011). The $^{40}Ar/^{39}Ar$ age of phengite from the high-P metamorphic belt is ~220 Ma (Zhai et al., 2011). This age is interpreted to represent the cooling event associated with crustal uplift in the region (Zhai et al., 2011).

3. Geology and petrography

The Jitang granite pluton is situated in the west side of Lancangjiang (Lancang River), ~3 km west of Jitang township, Changdu city (Fig. 2). The exposure of this pluton is about 70 km long and 2–10 km wide. The overall strike of the pluton is NNW. The immediate country rocks of the pluton belong to the Proterozoic Jitang group which is composed

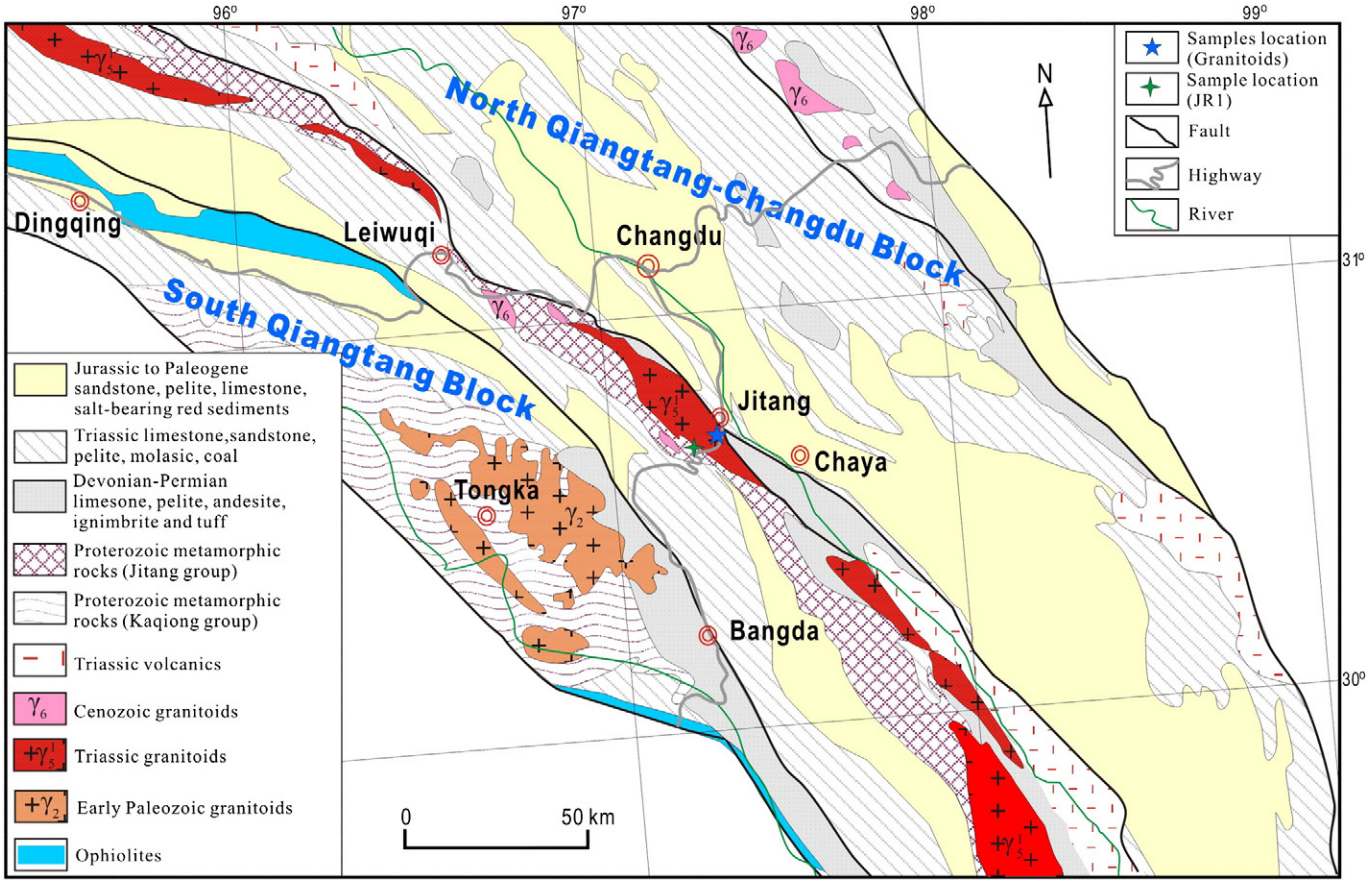

Fig. 2. Geological map of the Jitang area.
Modified from Pan et al. (2004).

of gneisses and amphibolite-facies meta-sedimentary rocks (Pan et al., 2004).

The Jitang pluton is mainly composed of medium-grained granodiorite and biotite granite. The contacts between different types of rocks are gradational. Biotite granite is porphyritic or equigranular (Fig. 3a and b). It contains 25–35 vol.% quartz, 30–40 vol.% K-feldspar plus perthite, 25–30 vol.% plagioclase, and 5–10 vol.% biotite. Accessory minerals include apatite, sphene, zircon, allanite and ilmenite. Granodiorite shows equigranular texture (Fig. 3c and d). It contains 20–30 vol.% quartz, 10–20 vol.% K-feldspar plus perthite, 35–45 vol.% plagioclase,

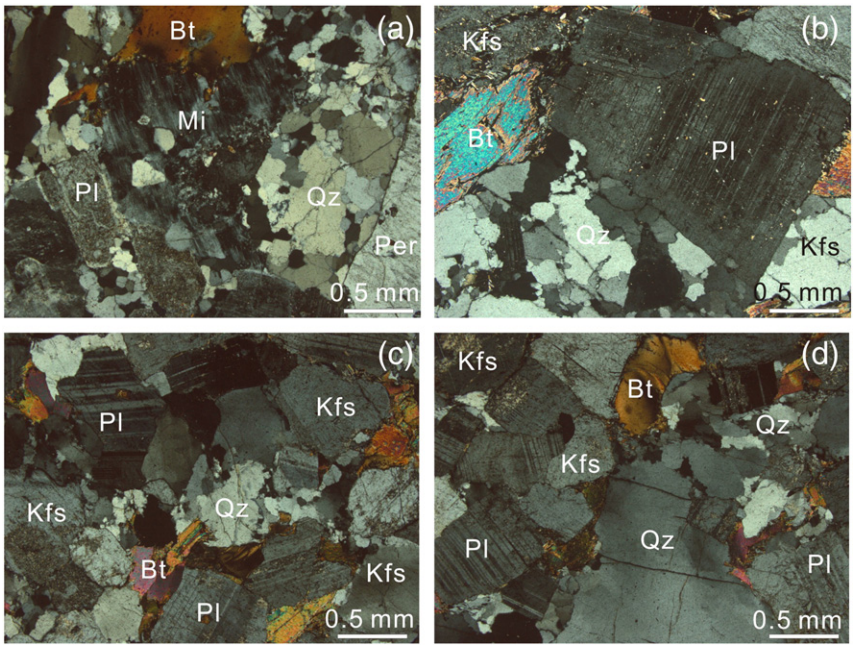

Fig. 3. Photomicrographs of biotite granites (a, b) and granodiorites (c, d) of the Jitang pluton. Qz, quartz; Pl, plagioclase; Kfs, K-feldspar; Per, perthite; Mi, microcline; Bt, biotite.

and 8–15 vol.% biotite. Accessory minerals are similar to that of biotite granite. The composition of plagioclase in granodiorite varies from oligoclase to andesine (An = l3–38). Polysynthetic twinning is common in tabular plagioclase grains. Quartz occurs as subhedral to anhedral grains in the interstitial spaces of the frameworks formed by plagioclase crystals. Biotite is anhedral and platy.

4. Sampling and analytical techniques

Samples were taken from outcrops along a highway near the Jitang township (Fig. 2). The major rock types of the Jitang pluton, such as granodiorite and biotite granite, are included in our sample collection. In addition, a gneiss sample from the Jitang group was also collected from a road cut in SW of the Jitang pluton (Fig. 2).

Whole-rock major element compositions were analyzed by XRF using an AXIOS-PW4400 instrument in the Institute of Geochemistry, Chinese Academy of Sciences, Guiyang. Whole-rock trace element abundances were determined by ICP-MS following the procedures of Qi et al. (2000).

Zircons in a large (8 kg) granite sample (JR3) were separated by heavy-liquid and magnetic separation, followed by hand-picking under a binocular microscope. More than 1000 zircon grains from the sample were found. The sizes of the zircons are 120–150 μm in length and 70–100 μm in width (Fig. 4). Most zircons are colorless and transparent, and have a prismatic morphology. They commonly show oscillatory zoning in cathodoluminescence images (Fig. 4).

Euhedral zircon crystals were selected using a binocular microscope. They were mounted in an epoxy disk and then polished. After Au-coating, the sample was loaded into a LEO1450VP scanning electron microscope for the collection of CL images. This was carried out at the Institute of Geology and Geophysics, Chinese Academy of Sciences, Beijing. Euhedral zircon crystals with clear oscillatory zoning in CL images were chosen for age determination.

U–Pb isotopic analyses of selected zircons were conducted using LA-ICP-MS in the State Key Laboratory of Ore Deposit Geochemistry, Institute of Geochemistry, Chinese Academy of Sciences, Guiyang. The instruments are a GeoLasPro laser-ablation system (Lambda Physik, Gottingen, Germany) and an Agilent 7700× ICP-MS (Agilent Technologies, Tokyo, Japan). A regulated 193 nm ArF excimer laser beam with a frequency of 10 J/cm^2 and a diameter of 32 μm was used. Each ablation took 40 s at 5 Hz repetition rate (equating to 200 pulses). Helium gas was used to transport the aerosol of zircon to the ICP-MS. The Zircon 91500 standard was used as external standard for instrument calibration. The zircon GJ-1 and Plešovice standards were used as reference materials. Lead concentration in zircon was external calibrated against NIST SRM 610 with Si as internal standard, while Zr as internal standard for other trace elements. Data reduction was performed using the ICPMSDataCal program from Liu et al. (2010). Plotting and age calculations are from Isoplot/Ex 3.00 (Ludwig, 2003).

Rb–Sr and Sm–Nd isotopic analyses of whole-rock samples were carried out using a Triton thermal ionization magnetic sector mass spectrometer in the Institute of Geochemistry, Chinese Academy of Sciences, Guiyang, using the procedures of Song et al. (2011). Mass fractionation corrections for Sr and Nd isotopic ratios were based on the values of $^{86}Sr/^{88}Sr = 0.1194$ and $^{146}Nd/^{144}Nd = 0.7219$.

5. Results

5.1. Zircon U–Pb age

The U–Pb data of 20 zircon grains selected from a granite sample (JR3) are listed in Table 1. In the concordia diagram, 14 of them plot close together and give a weighted mean $^{206}Pb/^{238}U$ age of 219.1 ± 1.7 Ma (Fig. 5). This age is interpreted to be the crystallization age of the Jitang pluton. The other six analyses have old $^{206}Pb/^{238}U$ ages from 295 Ma to 2293 Ma (Table 1). They are interpreted to be inherited or xenocrystic zircons.

5.2. Major elements

The major element abundances from the Jitang pluton are listed in Table 2. They contain 63.5–70.9 wt.% SiO_2, 2.8–4.2 wt.% Na_2O, 1.7–3.4 wt.% K_2O and 0.8–2.6 wt.% CaO. As mentioned above, the

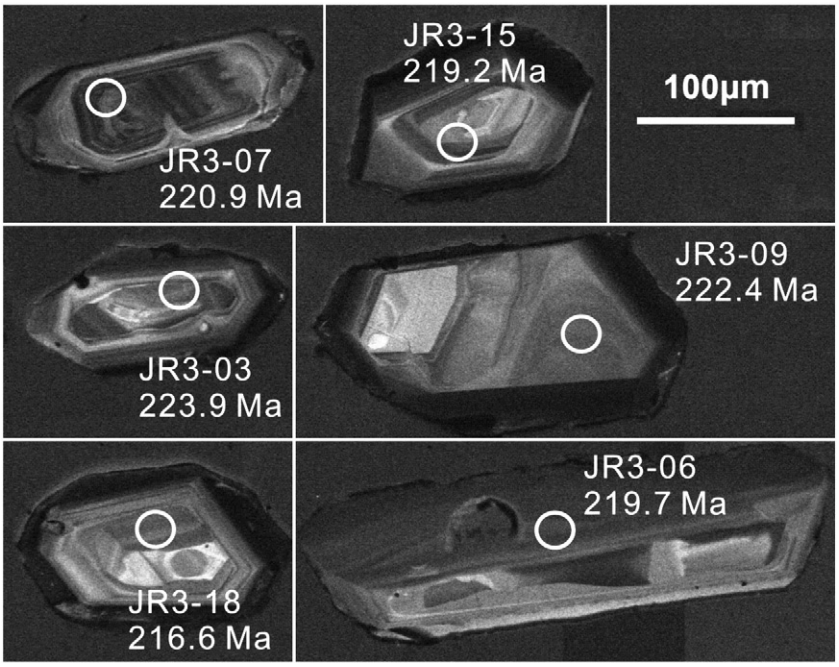

Fig. 4. Cathodoluminescence images of selected zircons from the Jitang pluton.

Table 1
LA-ICP-MS zircon U–Pb data for the Jitang pluton (GPS location of sample JR3: 30° 43′ 02″ N, 97° 20′ 25″ E).

Spot	Pb (Total)	Th (232)	U (238)	$^{207}Pb/^{235}U$		$^{206}Pb/^{238}U$		$^{208}Pb/^{232}Th$		$^{207}Pb/^{235}U$		$^{206}Pb/^{238}U$		$^{208}Pb/^{232}Th$		$^{208}Pb/^{232}Th$
	(ppm)	(ppm)	(ppm)	Ratio	1σ	Ratio	1σ	Ratio	1σ	Age (Ma)	1σ	Age (Ma)	1σ	Age (Ma)	1σ	
JR3-01	38.49	112	402	1.5724	0.0702	0.0903	0.0029	0.0353	0.0013	959.4	27.7	557.4	17.2	701.9		25.6
JR3-02	244.0	145	433	11.1072	0.1573	0.4271	0.0029	0.1190	0.0023	2532.2	13.2	2292.7	12.9	2273.4		41.8
JR3-03	18.26	200	466	0.2528	0.0043	0.0353	0.0003	0.0113	0.0002	228.8	3.5	223.9	1.6	227.8		4.1
JR3-04	22.90	287	573	0.2524	0.0038	0.0345	0.0002	0.0108	0.0002	228.5	3.1	218.8	1.5	217.3		3.7
JR3-05	21.87	212	550	0.2485	0.0040	0.0353	0.0003	0.0111	0.0002	225.4	3.3	223.9	1.6	222.5		3.9
JR3-06	17.80	76.5	495	0.2413	0.0037	0.0347	0.0002	0.0114	0.0003	219.4	3.0	219.7	1.5	229.1		6.1
JR3-07	42.7	571	1076	0.2507	0.0034	0.0349	0.0002	0.0113	0.0002	227.1	2.7	220.9	1.4	226.9		3.4
JR3-08	11.05	111	296	0.2494	0.0053	0.0352	0.0003	0.0110	0.0003	226.1	4.3	223.2	1.9	220.8		5.1
JR3-09	16.05	46.6	420	0.2465	0.0053	0.0351	0.0003	0.0101	0.0004	223.7	4.3	222.4	1.6	202.9		8.1
JR3-10	29.52	435	701	0.2406	0.0040	0.0342	0.0002	0.0106	0.0002	218.9	3.2	217.1	1.4	213.4		3.5
JR3-11	20.68	109	371	0.3364	0.0067	0.0467	0.0003	0.0204	0.0004	294.4	5.1	294.5	2.1	407.3		8.9
JR3-12	41.88	267	480	0.5497	0.0089	0.0701	0.0005	0.0226	0.0004	444.8	5.8	437.0	2.9	451.2		8.7
JR3-13	31.80	167	834	0.2415	0.0037	0.0344	0.0002	0.0109	0.0002	219.6	3.1	218.1	1.4	218.9		4.5
JR3-14	36.53	247	989	0.2414	0.0032	0.0339	0.0002	0.0110	0.0002	219.6	2.6	214.7	1.5	220.8		3.8
JR3-15	18.68	158	494	0.2366	0.0038	0.0346	0.0003	0.0106	0.0002	215.6	3.2	219.2	1.7	212.2		4.1
JR3-16	23.35	353	572	0.2403	0.0039	0.0340	0.0003	0.0108	0.0002	218.7	3.2	215.7	1.6	217.8		3.8
JR3-17	40.34	197	596	0.4586	0.0082	0.0587	0.0004	0.0189	0.0004	383.3	5.7	367.8	2.6	378.1		7.9
JR3-18	17.27	244	431	0.2522	0.0047	0.0342	0.0003	0.0110	0.0002	228.3	3.8	216.6	1.7	221.5		4.3
JR3-19	29.79	369	765	0.2449	0.0033	0.0342	0.0002	0.0104	0.0002	222.5	2.7	216.7	1.3	208.9		3.2
JR3-20	48.5	177	496	0.7390	0.0131	0.0815	0.0007	0.0366	0.0008	561.9	7.6	505.0	3.9	725.9		15.2

Jitang granitoids are classified as biotite granite and granodiorite based on modal mineral proportions. They all plot in the field of granodiorite (Fig. 6a) based on whole-rock SiO_2 and $Na_2O + K_2O$ contents (Middlemost, 1994). In the following presentation, data from the Lincang batholith, which has zircon U–Pb ages (Peng et al., 2013) similar to that of the Jitang pluton and occurs along the same tectonic suture as the Jitang pluton (see Fig. 1), are included for comparison. The Jitang and Lincang samples all plot significantly below the contour of Rittman index, $\sigma = 2.5$ which closely matches the division between subalkaline and alkaline series. The Lincang batholith and the Jitang pluton all belong to the peraluminous S-types (Fig. 6b and c). The zircon saturation temperatures of the Jitang pluton magma, calculated from the whole-rock compositions using the equation of Watson and Harrison (1983), vary between 740 and 850 °C (Table 2).

5.3. Trace elements

The trace element compositions of the Jitang granitoids are given in Table 2. The chondrite-normalized rare-earth element patterns and primitive mantle-normalized trace element patterns are illustrated in Fig. 7a and b. The slopes of the normalized patterns for the Jitang granitoids are similar to that of the average continental crust given in Rudnick and Gao (2003). Also, the Jitang granitoids show pronounced negative Eu–Ba–Nb–Sr–Ti anomalies, strikingly similar to the characteristics of the Indian cratonic basement (Célérier et al., 2009).

5.4. Sr–Nd isotopes

The Sr and Nd isotopic compositions of the Jitang pluton are given in Table 2. The Jitang granitoids have high initial $^{87}Sr/^{86}Sr$ ratios from 0.7266 to 0.7389 and low $\varepsilon_{Nd}(t)$ values from −11.1 to −13.2 (Fig. 8), which are similar to the values for the contemporaneous Lincang batholith (Hennig et al., 2009; Peng et al., 2013) but significantly lower than the values for slightly older andesites in the Lancangjiang volcanic belt (Peng et al., 2008). Compared to potential crustal source rocks, the isotopic compositions of the Jitang pluton are similar to that of a gneiss sample from the Jitang Group in the region, within the range of the Indian continental crust (gneisses plus Precambrian meta-sedimentary rocks) (Fig. 8). The calculated Nd isotopic model ages for the Jitang pluton are 2.0–2.3 Ga, similar to the model ages for the Lincang batholith (Hennig et al., 2009; Peng et al., 2013).

6. Discussion

6.1. Petrogenesis

S-type granites were inferred to have formed from a sedimentary source, such as meta-pelite or meta-greywacke (see summary in Brown, 2013). Experiments have shown that CaO/Na_2O ratio in a granitic melt is mainly controlled by source composition (Jung and Pfander, 2007). Melt derived from meta-pelite is characterized by CaO/Na_2O ratio <0.5. In contrast, melt derived from meta-greywacke has higher CaO/Na_2O ratio >0.3, with a mean of ~0.8 (Skjerlie and Johnston, 1996; Sylvester, 1998). The Jitang granitoids have CaO/Na_2O ratios close to 0.8, similar to melts derived from a meta-greywacke source. In the discrimination diagram of CaO/Na_2O versus Al_2O_3/TiO_2 ratios, all of the Jitang samples plot in the field of greywacke-derived melts (Fig. 9a). Greywacke-derived melts commonly have lower Rb/Ba and Rb/Sr ratios than pelite-derived melts (e.g., Harris and Inger, 1992; Miller, 1985). Based on Rb/Sr and Rb/Ba ratios, the Jitang granitoids plot within the field of greywacke-derived melts (Fig. 9b).

In felsic intrusive rocks, Sr and Eu are mainly hosted in plagioclase, whereas Ba is predominantly hosted in K-feldspar. The depletions of Eu and Sr, and to a lesser extent Ba, in the Jitang granitoids indicate

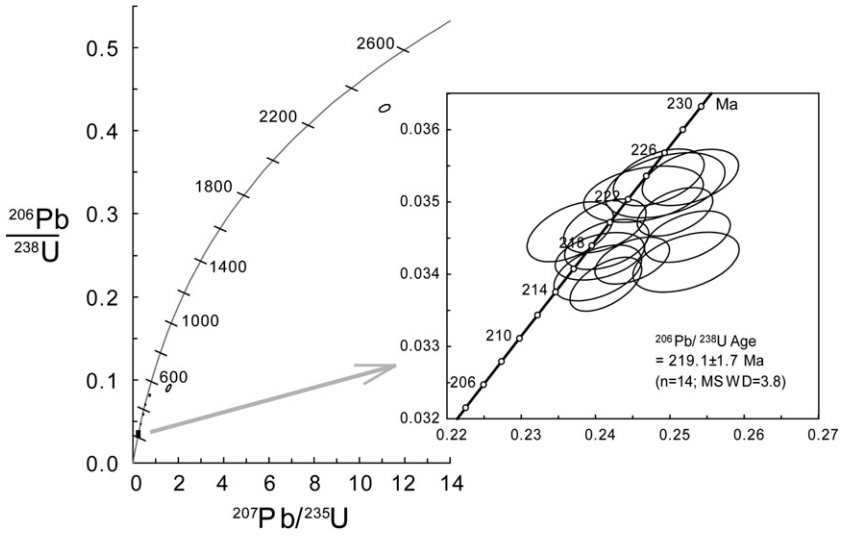

Fig. 5. Zircon U–Pb concordia diagram for the Jitang pluton.

that plagioclase and K-feldspar were important residual phases during partial melting. Using the solid–liquid partition coefficients for Rb, Sr and Ba from experiments (Icenhower and London, 1995, 1996; Nabelek and Bartlett, 1998; Nash and Crecraft, 1985), and the average composition of the bulk continental crust (Rudnick and Gao, 2003) as a starting composition, we have modeled the effects of different residual phases such as plagioclase, K-feldspar and biotite on the variations of these elements in the partial melts (Fig. 10). The results show that the compositional variations of the Jitang granitoids are generally consistent with 20–50% residual plagioclase in the source. The estimated values likely represent the maximum because the average Rb/Sr ratio in the real source of the Jitang pluton is likely much higher than that of the average continental crust from Rudnick and Gao (2003). As described above, the similarities between the Jitang granitoids and the Indian crust as well as the Jitang gneiss in trace element patterns (see Fig. 7a–b) and Sr–Nd isotopic compositions (see Fig. 8) indicate that the compositions of these crustal rocks are better choices to represent the source composition of the Jitang pluton than the average composition of global continental crust. Compared to the Indian cratonic basement gneisses and the Jitang gneiss, the Jitang granitoids show similar Rb/Sr ratios but lower Ba abundances (Fig. 10). The similarity and difference can be explained by <20% residual K-feldspar in a source with composition similar to that of the Indian cratonic basement and the Jitang gneiss.

The initial melting temperature of meta-greywacke is estimated to be 750–800 °C at the depth of ~20 km (Thompson, 1996). The zircon saturation temperatures in the Jitang magma estimated using the equation of Watson and Harrison (1983) are between 740 and 850 °C (Table 2), which are within the range of initial melting temperatures for meta-greywacke at the depth of ~20 km. However, the equation of Watson and Harrison (1983) was calibrated using partial melting experiments conducted at high pressures varying from 1.2 to 6 kbar. Based on the results from the experiments, total pressure does not have a significant effect on zircon saturation temperature (Watson and Harrison, 1983). Therefore, the depth of crustal anatexis at Jitang remains elusive.

6.2. Tectonic setting

The Jitang pluton occurs along the Longmu Co–Shuanghu suture (Fig. 1b) which formed by the closure of the ocean between the North and South Qiangtang blocks by oceanic subduction, followed by continental collision at 230–237 Ma as indicated by the U–Pb ages of zircons from high-grade metamorphic rocks of the suture zone (Zhai et al., 2011). The Ar–Ar ages of phengites from the high-grade metamorphic rocks are ~220 Ma, indicating that the exhumation took place before ~220 Ma (Zhai et al., 2011). The U–Pb age of zircons from the Jitang pluton (~219 Ma) indicates that this pluton was emplaced ~11–18 Ma after the event of high-pressure metamorphism in the suture.

Most of the samples from the Jitang pluton and the Lincang batholith plot in the field for granites formed in a late-collision to post-collision setting in the Hf–Rb/30–Ta × 3 tectonic discrimination diagram (Fig. 11), which is in general consistent with the geological constraints described above. Three of the samples plot within the field for granites formed in an arc setting. A reasonable explanation is more inputs from a juvenile arc crust for the outliers. Arc volcanic rocks such as basaltic andesites, andesites and rhyolites with zircon U–Pb ages varying from 248 to 275 Ma are present in the Zhaduo–Nangqian region (Yang et al., 2011) as well as in the Changdu region, north of the Longmu Co–Shuanghu suture (Fig. 1b). Subduction-related andesites with zircon U–Pb ages close to 248 Ma are abundant in the Lancangjiang volcanic belt (Peng et al., 2008), east of the Lincang batholith (Fig. 1b). The notion that juvenile arc crust may have played a minor role in the formation of the Jitang and Lincang S-type granitoids is also consistent with the Sr–Nd isotopic compositions of the related lithologies. The granitoids with lower initial $^{87}Sr/^{86}Sr$ ratios and higher $\varepsilon_{Nd}(t)$ values than the Jitang gneiss can be explained by <15% contribution from a juvenile arc crust (Fig. 8).

6.3. Implications for Gondwana reconstruction

The similarities in whole-rock elemental and Sr–Nd isotopic compositions between the Jitang and Lincang granitic plutons (Figs. 8 and 9) indicate that these two contemporaneous plutons share a common source. Triassic granitoids with Sr–Nd isotopic compositions similar to those of the Jitang and Lincang plutons are also present in South China (e.g., Wang et al., 2007). Thus, it is difficult to determine the origin of the source rocks by the isotopic data alone. The combination of the isotopic data with detrital zircon records is more useful. The age distribution patterns of detrital zircons from Simao-Indochina and North Qiangtang are strikingly different from that of detrital zircons from Yangtze craton but remarkably similar to that of detrital zircons from Tethyan Himalaya which has an Indian cratonic basement (He et al.,

Table 2
Major element compositions, trace element abundances and Sr–Nd isotopes of the Jitang pluton and associated country rock.

	Jitang pluton							Jitang group
Samples	JR2	JR3	JR4	JR5	JR6	JR7	JR8	JR1
Rock type	BG	BG	GD	GD	GD	GD	GD	Gneiss
SiO_2	68.73	70.87	66.74	65.66	62.80	67.61	63.45	68.22
TiO_2	0.65	0.57	0.75	0.74	0.58	0.62	0.67	0.75
Al_2O_3	14.78	14.20	15.09	15.27	14.57	15.87	15.16	13.27
Fe_2O_3	4.35	3.95	5.22	6.02	6.25	3.56	7.00	6.09
MnO	0.06	0.06	0.07	0.08	0.11	0.03	0.10	0.07
MgO	1.97	1.68	2.48	2.83	3.14	1.97	3.83	2.49
CaO	2.59	2.17	2.31	2.27	2.65	0.83	2.90	1.09
Na_2O	3.19	2.85	3.32	3.16	3.41	4.22	2.56	1.84
K_2O	2.88	3.39	2.76	2.82	2.76	2.12	1.75	2.42
P_2O_5	0.14	0.13	0.07	0.08	0.13	0.16	0.07	0.09
LOI	1.54	0.98	2.00	1.53	1.09	2.20	2.16	2.85
Total	100.89	100.84	100.81	100.47	97.49	99.19	99.64	99.18
Li	15.4	19.4	24.2	31.5	21.8	9.88	22.1	33.5
Be	3.02	2.47	1.86	1.49	1.36	4.87	4.73	3.11
Sc	11.7	11.6	13.2	19.1	17.1	13.7	18	14.2
V	71	64.5	82	93.7	79.5	70	113	108
Cr	42	38.6	74.3	78.8	86	41.7	122	82.5
Co	136	135	109	123	105	86.1	103	103
Ni	19	19.6	35.8	34.9	34.2	19.1	52.9	40.7
Cu	13.85	14.82	7.60	14.03	13.05	14.74	14.91	33.64
Zn	93.1	105	121	162	122	55.9	141	79.6
Ga	18.4	18.4	21.6	22.3	20.5	18.9	23.3	15.8
Ge	1.30	1.31	1.52	1.60	1.70	1.41	1.48	1.43
As	10.96	11.94	12.04	12.30	11.52	11.52	11.42	12.66
Rb	147	162	166	180	143	116	96.3	87.5
Sr	134	97.3	90	112	131	152	136	105
Y	27.1	30	66.1	48.9	35.4	30.3	16.1	27.3
Zr	139	105	171	153	99	229	153	127
Nb	16.5	11.8	15.6	16.1	9.85	12.4	8.66	12.3
Mo	0.48	1.30	0.35	0.42	0.37	0.25	0.49	0.36
Ag	0.496	0.425	0.479	0.59	0.342	0.389	0.309	0.435
Cd	0.309	0.257	0.351	0.327	0.264	0.172	0.22	0.15
In	0.076	0.075	0.096	0.101	0.154	0.060	0.090	0.06
Sn	5.38	4.91	5.05	3.73	5.35	3.83	3.31	3.62
Sb	1.70	1.19	1.22	1.38	0.96	1.03	13.06	2.06
Cs	4.46	4.64	4.25	5.3	3.69	1.36	2.72	5.80
Ba	458	469	249	333	538	697	540	719
La	45.1	47.5	62.9	54.5	68.3	54.1	43.2	32.3
Ce	86.5	94.1	124	110	145	105	86.2	65.2
Pr	9.84	11	14.6	13	16.9	12.1	10.1	7.46
Nd	35.1	40.5	52.9	47.3	62.5	43.7	36.9	27.4
Sm	7.15	8.29	11.6	9.8	12.7	8.12	7.22	5.9
Eu	1.00	0.85	1.05	1.08	1.24	1.11	1.27	1.22
Gd	6.18	7.95	11.64	10.29	12.09	7.12	6.64	5.40
Tb	1.07	1.16	1.88	1.57	1.73	1.13	0.868	0.894
Dy	5.51	5.93	10.9	8.52	7.9	5.6	3.49	5.08
Ho	1.07	1.16	2.36	1.78	1.42	1.12	0.614	1.10
Er	2.85	2.92	6.56	4.47	3.35	3.12	1.57	2.94
Tm	0.368	0.365	0.869	0.566	0.382	0.408	0.197	0.396
Yb	2.42	2.39	5.39	3.09	2.37	2.61	1.42	2.67
Lu	0.35	0.347	0.751	0.383	0.321	0.353	0.205	0.381
Hf	4.10	3.04	4.91	4.36	2.82	6.30	4.24	3.80
Ta	1.5	1.18	1.47	1.46	0.773	1.2	0.562	1.07
W	871	819	634	671	549	428	503	522
Tl	0.786	0.771	0.775	0.855	0.686	0.416	0.434	0.356
Pb	27.54	33.56	22.10	57.63	24.42	4.76	18.86	14.35
Bi	0.46	0.39	0.416	0.233	0.189	0.166	0.152	0.216
Th	25.5	28.3	43	35.3	47.4	28.4	23.8	14.7
U	2.3	2.73	2.99	2.38	1.8	2.3	1.8	2.2
T_{Zr} (°C)	777	758	797	789	738	847	795	
$^{87}Sr/^{86}Sr$	0.738668	0.748054	0.743193	0.741306	0.741628		0.745266	0.740191
$\pm 1\sigma$	0.000005	0.000005	0.000007	0.000007	0.000007		0.000008	0.000005
$^{87}Sr/^{86}Sr$ (i)	0.728804	0.733083	0.726608	0.726855	0.731812		0.738899	0.732697
$^{143}Nd/^{144}Nd$	0.511949	0.511965	0.511917	0.511917	0.511954		0.511849	0.511865
$\pm 1\sigma$	0.000002	0.000002	0.000003	0.000002	0.000002		0.000002	0.000001
$^{143}Nd/^{144}Nd$ (i)	0.511772	0.511787	0.511727	0.511737	0.511778		0.511679	0.511678
$\varepsilon_{Nd}(t)$	−11.39	−11.10	−12.28	−12.08	−11.29		−13.21	−13.23
T_{DM1} (Ma)	2018	2005	2311	2121	2003		2074	2340

BG, Biotite granite; GD, Granodiorite; T_{Zr}, zircon saturation temperature (calculated using the equation of Watson and Harrison, 1983); T_{DM1}, single-stage model age. $^{87}Sr/^{86}Sr_{(i,)}$, $^{143}Nd/^{144}Nd_{(i,)}$, and $\varepsilon_{Nd}(t)$ were calculated relative to present-day chondrite values (Jacobsen and Wasserburg, 1980), $^{143}Nd/^{144}Nd = 0.512638$, $^{147}Sm/^{144}Nd = 0.1967$, $^{87}Sr/^{86}Sr = 0.7045$ and $^{87}Rb/^{86}Sr = 0.0816$, λ (^{87}Rb) $= 1.42 \times 10^{-11}$ y^{-1}, λ (^{147}Sm) $= 6.54 \times 10^{-12}$ y^{-1}, and t = 219 Ma.

2011; Pullen et al., 2008; Usuki et al., 2012; Wang et al., 2013; Zhu et al., 2013). Based on the detrital zircon records, Zhu et al. (2013) and Wang et al. (2013) believed that the Simao-Indochina and North Qiangtang block were derived from the Indian Gondwana. The Sr–Nd isotopic compositions of the Jitang pluton in the North Qiangtang block and the Lincang batholith in the Simao-Indochina block (see Fig. 1b) are consistent with this interpretation. As shown in Fig. 8, the Sr–Nd isotopic compositions of these plutons are similar to those of the Indian cratonic crust. The occurrence of ~2.3 Ga inherited zircon in the Jitang pluton and the old Nd model ages (1.9–2.3 Ga) for the Jitang and Lincang plutons are also consistent with this interpretation.

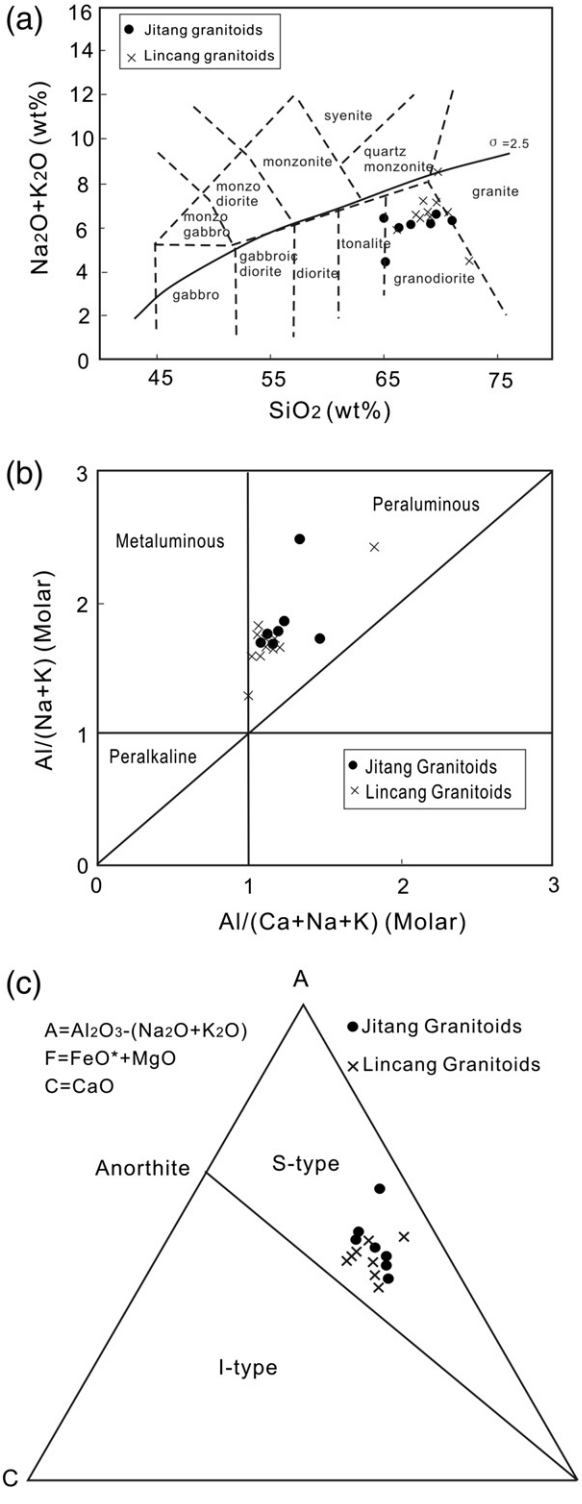

Fig. 6. (a) ($K_2O + Na_2O$) vs. SiO_2 (after Middlemost, 1994), with addition of a contour for $\sigma = 2.5$ [Rittman index, $\sigma = (K_2O + Na_2O)^2 / (SiO_2 - 43)$]. (b) Molar Al/(K + Na) vs. Al/(Ca + Na + K) (after Maniar and Piccoli, 1989). (c) ACF diagram (after Chappell and White, 1992). Whole rock compositions are corrected for loss-on-ignition. The data for the Lincang granitoids are from Dong et al. (2013).

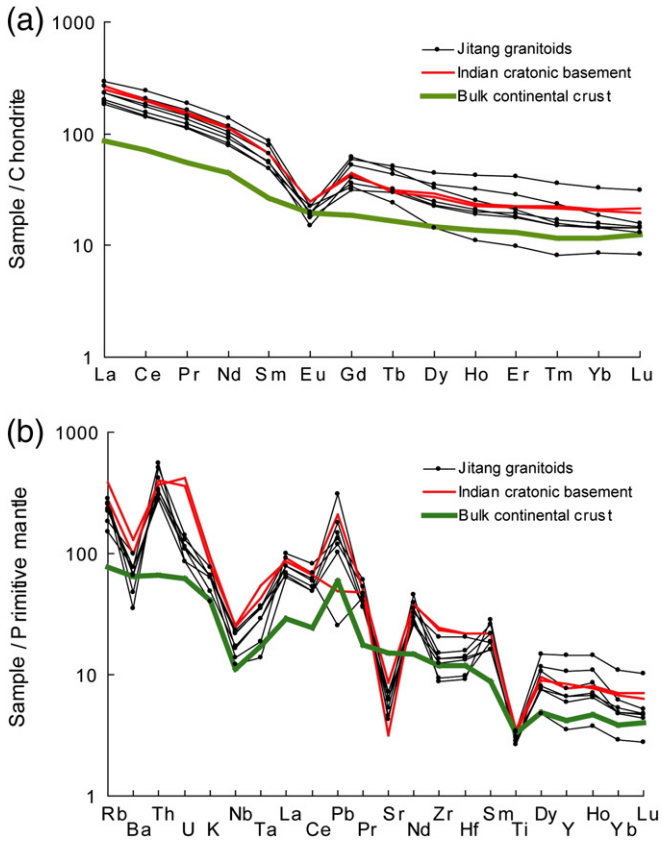

Fig. 7. Primitive mantle-normalized trace element patterns and chondrite-normalized rare-earth element patterns for the Jitang pluton. The primitive mantle values are from Sun and McDonough (1989). The chondrite values are from Anders and Grevesse (1989). The data for the continental crust are from Rudnick and Gao (2003). The data for the Indian cratonic basement (Ramgarh Group) are from Célérier et al. (2009).

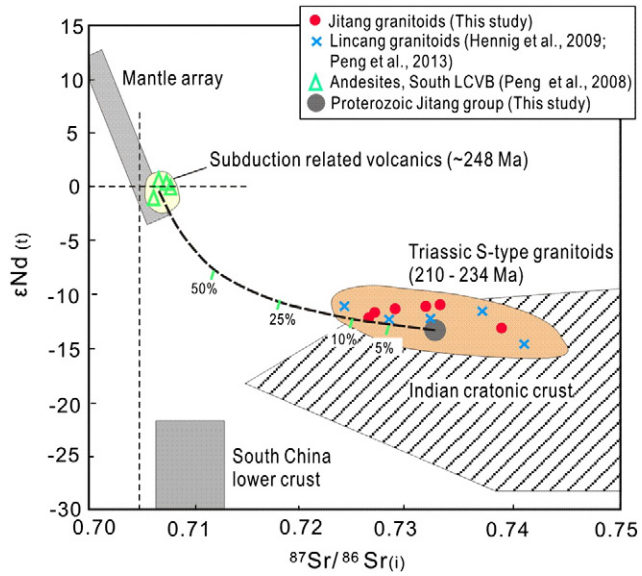

Fig. 8. Plot of $\varepsilon_{Nd}(t)$ vs. $(^{87}Sr/^{86}Sr)_i$. The mantle array is from Zindler and Hart (1986). The data for the lower crust of the South China block are from Chen and Jahn (1998). The data for the Indian cratonic crust (gneisses plus meta-sedimentary rocks >500 Ma) are from Ahmad et al. (2000), Richards et al. (2005), and references therein.

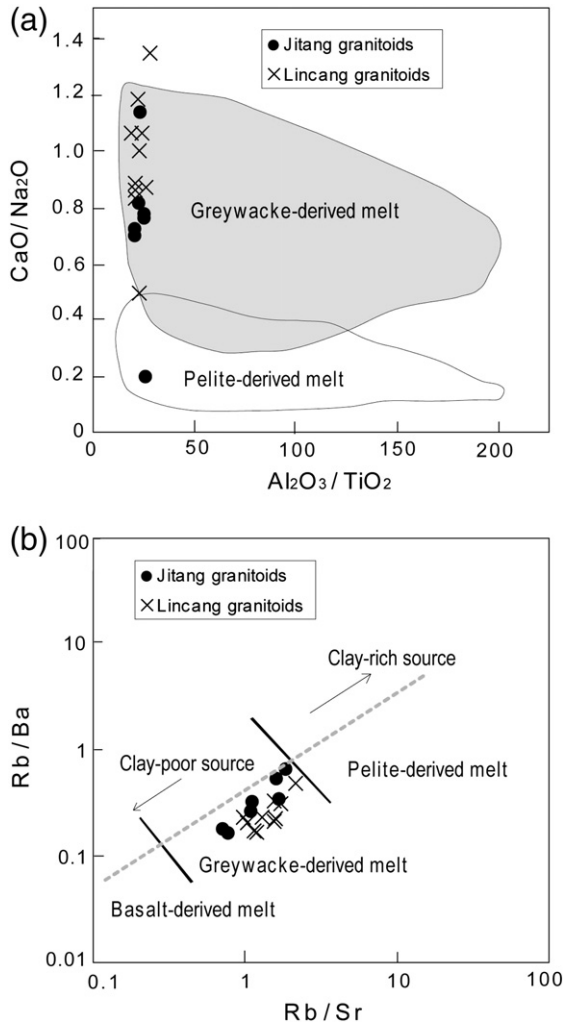

Fig. 9. Comparison of the Jitang S-type granitoids with partial melts of meta-pelite and meta-greywacke. The fields of different sources are from Jung and Pfander (2007), Patino Douce and Johnston (1991), and Sylvester (1998).

7. Conclusions

Important conclusions from this study are summarized below.

(1) The Jitang granitic pluton was emplaced at 219.1 ± 1.7 Ma in a post-collisional setting.

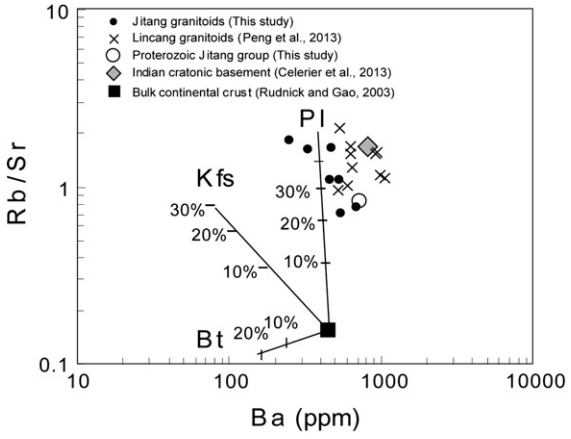

Fig. 10. Rb/Sr vs. Ba during partial melting. The solid–liquid partition coefficients used in the calculations are from Icenhower and London (1996, 1995), Nash and Crecraft (1985), and Nabelek and Bartlett (1998). *Pl*, plagioclase, *Kfs*, K-feldspar, *Bt*, biotite.

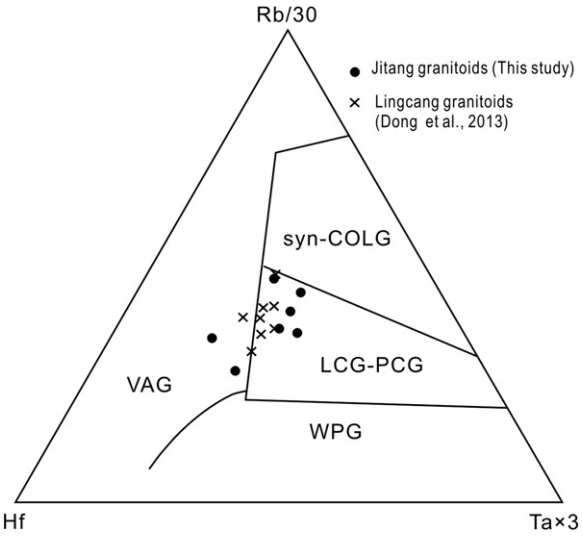

Fig. 11. Rb/30–Hf–Ta × 3 tectonic discrimination diagram (after Harris et al., 1986). VAG, volcanic arc granites, WPG, within-plate granites, syn-COLG, syn-collision granites, LCG, late-collision granites, PCG, post-collision granites.

(2) The Jitang pluton is a peraluminous, S-type pluton formed by crustal anatexis.
(3) The source of the pluton has Sr–Nd isotopes similar to those of the Indian cratonic crust.
(4) It is deduced that the North Qiangtang block was derived from the Indian Gondwana.

Conflict of interest

There is no conflict of interest.

Acknowledgments

We thank Jing Hu, Xiaobiao Li and Zhihui Dai of the State Key Laboratory of Ore Deposit Geochemistry, China for their assistance in trace element analysis, Sr–Nd isotope analysis and zircon U–Pb dating. We thank Prof. Nelsion Eby for revision guidance and two anonymous reviewers for constructive comments and useful suggestions. This study was supported by the National 973 Program of China (2009CB421005 and 2014CB440906), National Natural Sciences Foundations of China (41130423), and a grant from the State Key Laboratory of Ore Deposit Geochemistry of China (201202).

References

Ahmad, T., Harris, N., Bickle, M., Chapman, H., Bunbury, J., Prince, C., 2000. Isotopic constraints on the structural relationships between the Lesser Himalayan Series and the High Himalayan Crystalline Series, Garhwal Himalaya. Bulletin of the Geological Society of America 112, 467–477.
Anders, E., Grevesse, N., 1989. Abundances of the elements: meteoritic and solar. Geochimica et Cosmochimica Acta 53, 197–214.
Bi, X., Hu, R., Hanley, J.J., Mungall, J.E., Peng, J., Shang, L., Wu, K., Suang, Y., Li, H., Hu, X., 2009. Crystallization conditions (T, P, fO_2) from mineral chemistry of Cu- and Au-mineralized alkaline intrusions in the Red River-Jinshajiang alkaline igneous belt, western Yunnan province, China. Mineralogy and Petrology 96, 43–58.
Brown, M., 2013. Granite: from genesis to emplacement. Bulletin of the Geological Society of America 125, 1079–1113.
Burchfiel, B.C., Chen, Z., 2012. Tectonics of the southeastern Tibetan Plateau and its adjacent foreland. Geological Society of America Memoir 210, 231.
Célérier, J., Harrison, T.M., Webb, A.A.G., Yin, A., 2009. The Kumaun and Garwhal Lesser Himalaya, India: part 1. Structure and stratigraphy. Bulletin of the Geological Society of America 121, 1262–1280.
Chappell, B., White, A.J.R., 1992. I- and S-type granites in the Lachlan Fold Belt. Transactions of the Royal Society of Edinburgh, Earth Sciences 83, 1–26.
Chen, J., Jahn, B.-M., 1998. Crustal evolution of southeastern China: Nd and Sr isotopic evidence. Tectonophysics 284, 101–133.
Chen, F., Liu, C., Yong, Y., 1994. Granitoid and Cu–Sn–Au mineralization in eastern Xizang. Science Press, Beijing (197 pp. (in Chinese)).

Deng, J., Wang, Q., Li, G., Li, C., Wang, C., 2013. Tethys tectonic evolution and its bearing on the distribution of important mineral deposits in the Sanjiang region, SW China. Gondwana Research. http://dx.doi.org/10.1016/j.gr.2013.08.002.
Dong, G., Mo, X., Zhao, Z., Zhu, D., Goodman, R.C., Kong, H., Wang, S., 2013. Zircon U–Pb dating and the petrological and geochemical constraints on Lincang granite in Western Yunnan, China: implications for the closure of the Paleo-Tethys Ocean. Journal of Asian Earth Sciences 62, 282–294.
Fu, X.-G., Wang, J., Tan, F.-W., Chen, M., Chen, W.-B., 2010. The Late Triassic rift-related volcanic rocks from eastern Qiangtang, northern Tibet (China): age and tectonic implications. Gondwana Research 17, 135–144.
Harris, N.B.W., Inger, S., 1992. Trace element modeling of pelite derived granites. Contributions to Mineralogy and Petrology 110, 46–56.
Harris, N.B.W., Pearce, J.A., Tindle, A.G., 1986. Geochemical characteristics of collision-zone magmatism. In: Coward, M.P., Ries, A.C. (Eds.), Collision Tectonics. Special Publication, Geological Society of London, pp. 67–81.
He, S.P., Li, R.S., Wang, C., Zhang, H.F., Ji, W.H., Yu, P.S., Gu, P.Y., Shi, C., 2011. Discovery of 4.0 Ga detrital zircons in the Changdu Block, North Qiangtang, Tibetan Plateau. Chinese Science Bulletin 56, 647–658.
Hennig, D., Lehmann, B., Frei, D., Belyatsky, B., Zhao, X.F., Cabral, A.R., Zeng, P.S., Zhou, M.F., Schmidt, K., 2009. Early Permian seafloor to continental arc magmatism in the eastern Paleo-Tethys: U–Pb age and Nd–Sr isotope data from the southern Lancangjiang zone, Yunnan, China. Lithos 113, 408–422.
Icenhower, J., London, D., 1995. An experimental study of element partitioning among biotite, muscovite, and coexisting peraluminous silicic melt at 200 MPa (H_2O). American Mineralogist 80, 1229–1251.
Icenhower, J., London, D., 1996. Experimental partitioning of Rb, Cs, Sr, and Ba between alkali feldspar and peraluminous melt. American Mineralogist 81, 719–734.
Jacobsen, S.B., Wasserburg, G.J., 1980. Sm–Nd isotopic evolution of chondrites. Earth and Planetary Science Letters 50, 139–155.
Jian, P., Liu, D., Kröner, A., Zhang, Q., Wang, Y., Sun, X., Zhang, W., 2009. Devonian to Permian plate tectonic cycle of the Paleo-Tethys Orogen in southwest China (II): insights from zircon ages of ophiolites, arc/back-arc assemblages and within-plate igneous rocks and generation of the Emeishan CFB province. Lithos 113, 767–784.
Jung, S., Pfander, F.J.A., 2007. Source composition and melting temperatures of orogenic granitoids: constraints from CaO/Na_2O, Al_2O_3/TiO_2 and accessory mineral saturation thermometry. European Journal of Mineralogy 19, 859–870.
Li, G., Li, C., Ripley, E.M., Kamo, S., Su, S., 2012. Geochronology, petrology and geochemistry of the Nanlinshan and Banpo mafic–ultramafic intrusions: implications for subduction initiation in the eastern Paleo-Tethys. Contributions to Mineralogy and Petrology 164, 773–788.
Liang, H.-Y., Sun, W., Su, W.-C., Zartman, R.E., 2009. Porphyry copper–gold mineralization at Yulong, China, promoted by decreasing redox potential during magnetite alteration. Economic Geology 104, 587–596.
Liu, Y.S., Hu, Z.C., Zong, K.Q., 2010. Reappraisement and refinement of zircon U–Pb isotope and trace element analyses by LA-ICP-MS. Chinese Science Bulletin 55, 1535–1546.
Liu, Y., Santosh, M., Zhao, Z.B., Niu, W.C., Wang, G.H., 2011. Evidence for palaeo-Tethyan oceanic subduction within central Qiangtang, northern Tibet. Lithos 127, 39–53.
Ludwig, K.R., 2003. Using Isoplot/EX, version 3.0, A Geochronological Toolkit for Microsoft Excel. Berkeley Geochronological Center Special, Publication, No. 4.
Maniar, P.D., Piccoli, P.M., 1989. Tectonic discrimination of granitoids. Geological Society of America Bulletin 101, 635–643.
Metcalfe, I., 2002. Permian tectonic framework and palaeogeography of SE Asia. Journal of Asian Earth Sciences 20, 551–566.
Metcalfe, I., 2013. Gondwana dispersion and Asian accretion: tectonic and palaeogeographic evolution of eastern Tethys. Journal of Asian Earth Sciences. http://dx.doi.org/10.1016/j.jseaes.
Middlemost, E.A.K., 1994. Naming materials in the magma/igneous rock system. Earth Science Reviews 37, 215–224.
Miller, C.F., 1985. Are strongly peraluminous magmas derived from pelitic sedimentary sources? Journal of Geology 93, 673–689.
Nabelek, P.I., Bartlett, C.D., 1998. Petrologic and geochemical links between the post-collisional Proterozoic Harney Peak leucogranite, South Dakota, USA, and its source rocks. Lithos 45, 71–85.
Nash, W.P., Crecraft, H.R., 1985. Partition coefficients for trace elements in silicic magmas. Geochimica et Cosmochimica Acta 49, 2309–2322.
Pan, G., Ding, J., Yao, D., Wang, L., 2004. Geological Map of Qinghai-Xizang (Tibet) Plateau and Adjacent Areas (1:1500000). Chengdu Cartographic Publishing House, Chengdu, China.
Patino Douce, A.E., Johnston, A.D., 1991. Phase equilibria and melt productivity in the pelitic system: implications for the origin of peraluminous granitoids and aluminous granulites. Contributions to Mineralogy and Petrology 107, 202–218.
Peng, T., Wang, Y., Fan, W., Liu, D., Shi, Y., Miao, L., 2006. SHRIMP zircon U–Pb geochronology of Early Mesozoic felsic igneous rocks from the southern Lancangjiang and its tectonic implications. Science in China (Series D) 49, 1032–1042.
Peng, T., Wang, Y., Zhao, G., Fan, W., Peng, B., 2008. Arc-like volcanic rocks from the southern Lancangjiang zone, SW China: geochronological and geochemical constraints on their petrogenesis and tectonic implications. Lithos 102, 358–373.
Peng, T., Wilde, S.A., Wang, Y., Fan, W., Peng, B., 2013. Mid-Triassic felsic igneous rocks from the southern Lancangjiang Zone, SW China: petrogenesis and implications for the evolution of Paleo-Tethys. Lithos 168–169, 15–32.
Pullen, A., Kapp, P., Gehrels, G.E., Vervoort, J.D., Ding, L., 2008. Triassic continental subduction in central Tibet and Mediterranean-style closure of the Paleo-Tethys Ocean. Geology 36, 351–354.
Qi, L., Hu, J., Grégoire, D.C., 2000. Determination of trace elements in granites by inductively coupled plasma mass spectrometry. Talanta 51, 507–513.
Qiangba, Z.-X., Xie, Y.-W., Wu, Y.-W., Xie, C.-M., Li, Q.-L., Qiu, J.-Q., 2009. Zircon SIMS U–Pb dating and its significance of cumulate gabbro from Dengqen ophiolite, eastern Tibet, China. Geological Bulletin of China 28, 1253–1259 (in Chinese with English abstract).
Richards, A., Argles, T., Harris, N., Parrish, R., Ahmad, T., Darbyshire, F., Draganits, E., 2005. Himalayan architecture constrained by isotopic tracers from clastic sediments. Earth and Planetary Science Letters 236, 773–796.
Rudnick, R.L., Gao, S., 2003. Composition of the continental crust. In: Rudnick, R.L. (Ed.), Treatise on Geochemistry. The Crust, vol. 3. Elsevier, pp. 1–64.
Shi, R.D., 2007. SHRIMP dating of the Bangong Lake SSZ-type ophiolite: constraints on the closure time of ocean in the Bangong Lake–Nujiang River, northwestern Tibet. Chinese Science Bulletin 52, 936–941.
Skjerlie, K.P., Johnston, A.D., 1996. Vapour-absent melting from 10 to 20 kbar of crustal rocks that contain multiple hydrous phases: implications for anatexis in the deep to very deep continental crust and active continental margins. Journal of Petrology 37, 661–691.
Song, X.-Y., Xie, W., Deng, Y.-F., Crawford, A.J., Zheng, W.-Q., Zhou, G.F., Deng, G., Cheng, S.-L., Li, J., 2011. Slab break-off and the formation of Permian mafic–ultramafic intrusions in southern margin of Central Asian Orogenic Belt, Xinjiang, NW China. Lithos 127, 128–143.
Sun, S.-S., McDonough, W.F., 1989. Chemical and isotopic systematics in ocean basalt: implication for mantle composition and processes. In: Saunders, A.D., Norry, M.J. (Eds.), Magmatism in the Ocean Basins. Geological Society of London Special Publications, 42, pp. 313–345.
Sylvester, P.J., 1998. Post-collisional strongly peraluminous granites. Lithos 45, 29–44.
Thompson, A.B., 1996. Fertility of crustal rocks during anatexis. GSA Special Papers 315, 1–10.
Usuki, T., Lan, C.Y., Wang, K.L., Chiu, H.Y., 2012. Linking the Indochina craton and Gondwana during the Early Paleozoic: evidence from U–Pb ages and Hf isotopes of detrital zircons. Tectonophysics 586, 145–159.
Wang, Y., Fan, W., Sun, M., Liang, X., Zhang, Y., Peng, T., 2007. Geochronological, geochemical and geothermal constraints on petrogenesis of the Indosinian peraluminous granites in the South China Block: a case study in the Hunan Province. Lithos 96, 475–502.
Wang, W.-L., Aitchison, J.C., Lo, C.-H., Zeng, Q.-G., 2008. Geochemistry and geochronology of the amphibolite blocks in ophiolitic mélanges along Bangong–Nujiang suture, central Tibet. Journal of Asian Earth Sciences 33, 122–138.
Wang, Y., Zhang, A., Fan, W., Peng, T., Zhang, F., Zhang, Y., Bi, X., 2010. Petrogenesis of late Triassic post-collisional basaltic rocks of the Lancangjiang tectonic zone, southwest China, and tectonic implications for the evolution of the eastern Paleotethys: geochronological and geochemical constraints. Lithos 120, 529–546.
Wang, Q., Deng, J., Li, C., Li, G., Li, Y., Qiao, L., 2013. The boundary between the Simao and Yangtze blocks and their locations in Gondwana and Rodinia: constraints from detrital and inherited zircons. Gondwana Research. http://dx.doi.org/10.1016/j.gr.2013.10.002.
Watson, E.B., Harrison, T.M., 1983. Zircon saturation revisited: temperature and composition effects in a variety of crustal magma types. Earth and Planetary Science Letters 64, 295–304.
Yang, T.N., Zhang, H.R., Liu, Y.X., Wang, Z.L., Song, Y.C., Yang, Z.S., Tian, S.H., Xie, H.Q., Hou, K.J., 2011. Permo-Triassic arc magmatism in central Tibet: evidence from zircon U–Pb geochronology, Hf isotopes, rare earth elements, and bulk geochemistry. Chemical Geology 284, 270–282.
Yin, A., Harrison, T.M., 2000. Geologic evolution of the Himalayan–Tibetan orogen. Annual Review of Earth and Planetary Sciences 28, 211–280.
Zhai, Q.-G., Zhang, R.-Y., Jahn, B.-M., Li, C., Song, S.-G., Wang, J., 2011. Triassic eclogites from central Qiangtang, northern Tibet, China: petrology, geochronology and metamorphic P–T path. Lithos 125, 173–189.
Zhai, Q.-G., Jahn, B.-M., Su, L., Wang, J., Mo, X.-X., Lee, H.-Y., Wang, K.-L., Tang, S., 2013. Triassic arc magmatism in the Qiangtang area, northern Tibet: Zircon U–Pb ages, geochemical and Sr–Nd–Hf isotopic characteristics, and tectonic implications. Journal of Asian Earth Sciences 63, 162–178.
Zhang, Y.-C., Shi, G.R., Shen, S.-Z., 2013. A review of Permian stratigraphy, palaeobiogeography and palaeogeography of the Qinghai–Tibet Plateau. Gondwana Research 24, 55–76.
Zhu, J.-J., Hu, R.-Z., Bi, X.-W., Zhong, H., Chen, H., 2011. Zircon U–Pb ages, Hf–O isotopes and whole-rock Sr–Nd–Pb isotopic geochemistry of granitoids in the Jinshajiang suture zone, SW China: constraints on petrogenesis and tectonic evolution of the Paleo-Tethys Ocean. Lithos 126, 248–264.
Zhu, D.-C., Zhao, Z.-D., Niu, Y., Dilek, Y., Hou, Z.-Q., Mo, X.-X., 2013. The origin and pre-Cenozoic evolution of the Tibetan Plateau. Gondwana Research 23, 1429–1454.
Zi, J.-W., Cawood, P.A., Fan, W.-M., Tohver, E., Wang, Y.-J., McCuaig, T.C., 2012a. Generation of Early Indosinian enriched mantle-derived granitoid pluton in the Sanjiang Orogen (SW China) in response to closure of the Paleo-Tethys. Lithos 140–141, 166–182.
Zi, J.-W., Cawood, P.A., Fan, W.-M., Wang, Y.-J., Tohver, E., McCuaig, T.C., Peng, T.-P., 2012b. Triassic collision in the Paleo-Tethys Ocean constrained by volcanic activity in SW China. Lithos 144–145, 145–160.
Zi, J.-W., Cawood, P.A., Fan, W.-M., Tohver, E., Wang, Y.-J., McCuaig, T.C., Peng, T.-P., 2013. Late Permian-Triassic magmatic evolution in the Jinshajiang orogenic belt, SW China and implications for orogenic processes following closure of the Paleo-Tethys. American Journal of Science 313, 81–112.
Zindler, A., Hart, S.R., 1986. Chemical geodynamics. Annual Review of Earth and Planetary Sciences 14, 493–571.